scientific reports

Check for updates

OPEN

Amplitude only nulling of linear antenna arrays for 5G/6G wireless communication by using honey formation optimization

Ali Akdagli[1], Ali Yildiz[1], Filiz Karaomerlioglu[1], Gökhan Yüksek[2], Serdar Ekinci[3], Davut Izci[4]✉, Mostafa Rashdan[5]✉ & Mohammad Salman[5]

This paper presents a new pattern nulling method for linear antenna arrays using the honey formation optimization with a single component (HFOSC) algorithm. HFOSC was validated through extensive tests on 60 benchmark functions, demonstrating superior accuracy and convergence compared to particle swarm optimization (PSO), differential search (DS), moth-flame optimization (MFO), whale optimization algorithm (WOA), and improved grey wolf optimizer (IGWO). The proposed method enables accurate null steering by adjusting only the amplitudes of the array's individual elements while keeping uniform phase and position distributions for a fixed array geometry. A compound cost function including sidelobe levels, null depths, and dynamic range ratios is defined with customized weighting coefficients for the optimization. The HFOSC algorithm performance and feasibility are demonstrated elaborately through illustrative and total numerical simulations based on a 25-element linear array spaced by half-wavelength operating at 28 GHz. The array is synthesized with a 25-dB Chebyshev pattern under single, multiple, and wide null constraints. The simulation results always demonstrate that the proposed optimizer is capable of generating solutions satisfying such contradictory pattern requirements as well as stringent interference suppression constraints to ensure Quality of Service (QoS) and enhance user satisfaction. Thus, this technique is very promising for applications in evolving 5G/6G communication systems.

Keywords Linear antenna array, Pattern nulling, Null steering, Honey formation optimization

The next generation 6G wireless networks are expected to have even more stringent requirements on capacity, coverage, latency, and reliability. To satisfy them, it is compulsory to exploit heterogeneous antenna structures with advanced beamforming. A major design objective is to synthesize patterns with high-gain primary lobes that are capable of achieving tight and deep nulls in the directions of interferers, which is required for cognitive radios that perform dynamic spectrum access and interference suppression in strongly interfered spectrum bands. The achievement of such a system relies heavily on advanced antenna arrays to provide intelligent spatial resource sharing, including dynamic beam steering, interference avoidance, and concentrated signal transmission. While linear arrays are fundamental building blocks due to their simplicity and their ability to precisely control the beam, their use in high-density 6G networks is hindered by major challenges such as mutual coupling between closely spaced elements, degrading the pattern performance as well as the nulling accuracy if not taken into consideration[1–4].

The antenna arrays are essential components of 5G/6G infrastructure, particularly for base stations. They enable dramatic increases in network capacity and link data rates while mitigating inter-user interference. In parallel, the research on antenna pattern synthesis has been hurried up due to the fact that the electromagnetic spectrum has been increasingly overcrowded, especially on the problem of deep null generation in some pre-specified directions[5–19]. These are important techniques for wireless communication system, radar and sonar systems to avoid diminishing SNR due to co-channel interference and jamming. In addition, there are more

[1]Department of Electrical and Electronics Engineering, Mersin University, Mersin, Turkey. [2]Department of Electrical and Electronics Engineering, Batman University, Batman, Turkey. [3]Department of Computer Engineering, Bitlis Eren University, Bitlis 13100, Turkey. [4]Department of Electrical and Electronic Engineering, Bursa Uludag University, Bursa 16059, Turkey. [5]College of Engineering and Technology, American University of the Middle East, Egaila 54200, Kuwait. ✉email: davutizci@uludag.edu.tr; mostafa.rashdan@aum.edu.kw

and more demands for radiation pattern with larger null regions extension[7,10]. Such wide nulls are especially important in cases of interferers with unknown or time-dependent directions of arrival as narrow nulls would have to be continuously adjusted in real-time to maintain system performance.

Conventional null steering methods reported in the literature for the above can be classified according to the manipulated array parameter. They can be viewed as the complex weighting (amplitude and phase) of the excitation, or only the excitation amplitude or phase can be controlled separately, or the physical position of the antenna elements in the array can be changed. The overall goal is still to maintain the main lobe gain in the direction of the signal of interest while forcing nulls in the direction of interferers. Amplitude-only control realized by means of attenuator networks is a very powerful and simple method providing the easiest integration in hardware and great operational efficiency[2,5,10,11]. This method is excellent for robust null placement with low computational burden, which makes it particularly good for real-time and low power consumption applications. Conversely, phase-only[10,11,16,19], position-only[12–14] control, and the like, lead to the more difficult nonlinear optimization problems, which usually cannot be solved analytically. Although it is possible to linearize for small phase disturbances, this simplification is often too restrictive to allow nulls to be placed symmetrically about the main beam. In fact, displacing element positions can produce symmetric null placement, but at the potential cost of practicality since it requires mechanical actuation systems such as servomotors for real time adjustment. The amplitude only method is especially attractive for phased arrays as the well-known attenuator networks can be used to accomplish the nulling without investment in additional phase shifting hardware and hence with minimum growth in cost, improved reliability, and seamless scalability to very high density 6G networks[1,2].

Building on these traditional null steering techniques, which mainly involve modifying array element parameters such as amplitudes, phases, or positions in order to achieve interference suppression, the direct synthesis of optimal radiation patterns is typically carried out using advanced optimization formulations. The performance disparity between the development of a nulling algorithm and the practical computation of its parameters has motivated investigations into more powerful and intelligent numerical methods. Traditionally, this has been addressed through analytical or gradient-based numerical approaches. Nevertheless, these traditional solvers are not well suited to handle the non-convex and multi-modal cost functions encountered when synthesizing patterns with multiple, deep nulls simultaneously. Standard gradient-based methods are often limited by the need for a good initial guess, which is not always readily available. Without a sufficiently close starting point to the global optimum, these methods tend to converge toward local minimizers, which may be suboptimal. This constraint becomes increasingly important as the size of the parameter space increases, since the quality of the solution depends heavily on the initial guess. To tackle these issues, Artificial Intelligence (AI) driven metaheuristic optimization techniques have been extensively employed to solve challenging antenna design problems[20–33]. Methods such as genetic algorithms (GA), particle swarm optimization (PSO), and grey wolf optimization (GWO) and more have proven to be effective in nonlinear engineering problems, with particular trade-offs in terms of exploration, exploitation, and computational overhead[28–37].

Another recently developed member of the family of nature-inspired heuristics is honey formation optimization (HFO), which simulates the gradual maturation of honey in a beehive[38–40]. The classical HFO was developed as a multi-component model. A further simplification led to a single-component version, named HFO-1, in which all candidate solutions evolve independently[39]. For convenience, this variant is referred to herein as honey formation optimization with single component (HFOSC). The HFOSC method was thoroughly tested against 60 benchmark test functions. The findings illustrate that HFOSC achieves better results than well-known metaheuristics, including PSO, Differential Search (DS), Moth-Flame Optimization (MFO), Whale Optimization Algorithm (WOA), and the Improved Grey Wolf Optimizer (IGWO), in terms of solution accuracy and convergence rate[40]. Compared to existing metaheuristic methods, HFOSC offers three key practical advantages: (i) significantly faster convergence owing to its maturation-triggered saturation mechanism, (ii) improved solution stability across independent runs as evidenced by the lowest standard deviation among all compared algorithms, and (iii) effective dynamic range ratio (DRR) control through the weighted cost function, which facilitates hardware-feasible amplitude distributions.

In this paper, the HFOSC is utilized to synthesize linear antenna arrays with amplitude-only control. The problem of optimization is posed in terms of a suitable cost function including the null depth, maximum sidelobe level, and the dynamic range of the excitation amplitudes, weighted according to the design priorities. By allowing only amplitude variation and holding phase values fixed, the method obtains rigorous null placement with practical implementation. Extensive numerical simulations performed with a 25-element linear array with half wavelength spacing at 28 GHz demonstrate the feasibility of the 25-dB Chebyshev radiation pattern synthesis with additional constraints for single, multiple, and broad null patterns. The results indicate that the proposed algorithm can be directly employed to achieve high suppression accuracy while maintaining a favorable trade-off among sidelobe, null depth, and dynamic range. Moreover, HFOSC emerges as a general-purpose technique for high-dimensional and strongly non-convex antenna pattern synthesis design problems, offering a substantial reduction in computational burden, even in multi-objective synthesis scenarios. These characteristics make the method well suited for interference suppression and anti-jamming in future wireless applications, including 6G communication systems.

Formulation

If elements are linearly symmetric about the center element of an array antenna, the far-field array factor for an array with an odd number of isotropic elements $(2N+1)$ can be expressed as:

$$AF(\theta) = \sum_{n=-N}^{N} a_n e^{jnkd_n \sin(\theta)} \quad , -90^o \leq \theta \leq 90^o \tag{1}$$

Here, d_n signifies the distance from the central element of the array to the position of the n_{th} element, while a_n denotes its corresponding amplitude. k is the wavenumber, which equals $2\pi / \lambda$, where λ represents the wavelength. θ is the angle measured from the axis perpendicular (broadside direction) to the linear array antenna. In this work, the synthesis is performed using the array-factor model with isotropic elements, uniform phase, and fixed inter-element spacing. This formulation neglects mutual coupling and element pattern variations, which may affect the realized null depths and sidelobe levels in practical arrays.

The optimization procedure additionally incorporates essential design parameters such as the null depth level (NDL), maximum sidelobe level (MSL), and dynamic range ratio (DRR). These parameters are integrated into a cost function through specific weighting coefficients, which are presented as follows:

$$C = |AF_o(\theta) - AF_d(\theta)| + w_1 ENDL + w_2 EMSL + w_3 DRR \tag{2}$$

where $AF_o(\theta)$, $AF_d(\theta)$, $ENDL$, and $EMSL$ denote, respectively, the obtained pattern and the desired pattern, the error of the NDL, and the error of the MSL. The DRR equals $|a_{max}/a_{min}|$, where a_{max} and a_{min} are the maximum and minimum amplitude values of the elements, respectively. The weighting parameters w_1, w_2, and w_3 are to be selected based on empirical knowledge so that the cost function can guide the candidate solutions closer to the optimal one. This ensures the resulting array pattern has the desired performance. To achieve the desired radiation pattern with predetermined nulling directions, the cost function defined in Eq. (2) is minimized using the proposed HFOSC algorithm, which is explained in the following section.

Honey Formation Optimization with Single Component (HFOSC)

HFOSC is a single-population evolutionary algorithm in which each individual solution evolves on its own without coordination among multiple sources[39,40]. It simulates the honey ripening process via three mixing phases: Mixing-0 (exploration), Mixing-1 (semi-mature refinement), and Mixing-2 (mature exploitation). The procedure iterates solution updates, maturation testing, and best global solution (BGS) based convergence acceleration, providing a balance between exploration and exploitation.

Figure 1 shows the flowchart of HFOSC. The algorithm also includes explicit phases of maturation and saturation. Stability is watched by comparing the convergence of fitness values of consecutive generations; when a solution converges, that solution is perceived to be mature and the algorithm goes to saturation stage to speed up convergence. When the saturation process begins, the BGS is used as the seeds to be mixed into the population with the idea that better candidates should take the lead in influencing the searching process rather than being lost owing to greed. This dynamic adjustment mechanism can avoid the premature convergence and balance the exploration-exploitation.

The detailed implementation of maturity detection and BGS catalysis is given below.

1. Initialize population X randomly within bounds; evaluate fitness f(x_i).
2. Identify BGS = argmin f(x_i).
3. For t = 1 to T (max iterations):

For each individual x_i in X:
Apply Mixing-0, Mixing-1, Mixing-2 sequentially.
Apply bound repair; evaluate f(x_i).
// Maturity detection.
For each x_i:
If |f(x_i, t) - f(x_i, t-k)| < ε then mark x_i as mature.
// BGS catalysis.
Replace the worst-performing mature individuals with perturbed BGS:
x_new = BGS + η · randn().
Apply bound repair; evaluate new individuals.
Update BGS if a better solution is found.

4. Return BGS and f(BGS)

Here, k is the number of consecutive generations for maturity detection (e.g., k = 5), ε is a small tolerance (e.g., 10^{-6}), and η is a small perturbation amplitude (e.g., 0.01 × variable range).

Numerical examples and results

To comprehensively assess the proposed amplitude-only nulling method, the HFOSC algorithm was employed to synthesize patterns for a 25-element linear array. The array operates at 28 GHz with a half-wavelength inter-element spacing ($d = \lambda/2$). The reference pattern is a 25-dB Chebyshev distribution, as shown in Fig. 2. Seven distinct nulling examples, encompassing single, multiple, and broad nulls, were optimized, with key performance metrics (NDL, MSL and DRR).

As a first example, the desired array factor $AF_d(\theta)$ is defined in an angle-specific, piecewise manner to localize suppression to the critical sidelobe only. The nulling angle, denoted by θ_{na}, corresponds to 15.5°, which marks the angular location of the third sidelobe. Specifically:

1. **Initialization**
   - Define the optimization problem, design variables, and bounds.
   - Set algorithm parameters (population size, maximum iterations, tolerance).
   - Randomly generate the initial population of candidate solutions and evaluate the objective (cost) function.
2. **Global Best Identification**
   - Select the candidate with the minimum cost as the**Best Global Solution (BGS)**.
3. **Iterative Improvement (Main Loop)**
   - **Repeat until a stopping criterion is met**(maximum iterations or target cost):

   3.1. **Mixing Stages (Solution Update)**
   - Update each candidate solution**independently**(single-component search).
   - Apply sequential mixing operators:
     - **Mixing-0:**initial exploratory perturbation to generate new trial solutions.
     - **Mixing-1:**refinement of semi-mature solutions via structured mixing.
     - **Mixing-2:**intensified exploitation to further improve mature solutions.

   3.2. **Feasibility and Evaluation**
   - Enforce variable bounds (repair/clipping if necessary).
   - Recompute the objective (cost) function for updated candidates.

   3.3. **Maturation Check**
   - Monitor fitness improvement; if no significant improvement is observed over consecutive iterations, mark the candidate as**mature**.

   3.4. **Saturation and BGS Catalysis**
   - When saturation is detected, inject or use**BGS as a catalyst**to accelerate convergence while maintaining population diversity.

   3.5. **BGS Update**
   - If a better candidate is found, update**BGS**accordingly.
4. **Termination**
   - Output**BGS**as the optimized solution (e.g., amplitude set) and report performance metrics (e.g., null depth, sidelobe level, DRR).

Fig. 1. The flow chart of HFOSC algorithm.

$$AF_d(\theta) = \begin{cases} 0, \text{if } \theta = \theta_{na} \\ \text{Initial Chebyshev pattern, otherwise} \end{cases} \tag{3}$$

This selective definition ensures that only the sidelobe at 15.5° is targeted for modification, while the rest of the pattern maintains high similarity to the initial Chebyshev pattern. To avoid penalizing patterns that already achieve sufficient suppression at the nulling direction, a threshold condition is incorporated into the cost function:

$$ENDL = \begin{cases} 0, & if\ AF_o(\theta_{na}) \leq NDL \\ 1, & \text{otherwise} \end{cases} \tag{4}$$

The NDL is chosen as -90 dB to ensure a sufficiently high degree of suppression for most practical antenna applications. This prevents unnecessary penalization in the cost function when the desired suppression has already been reached. To avoid the levels of sidelobe increases, the following EMSL function is applied only for angular positions outside of the main lobe, which starts from 6° in the current pattern.

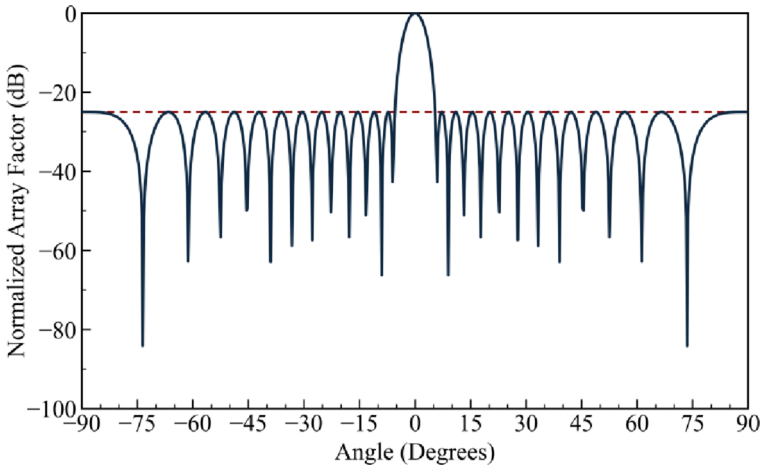


Fig. 2. The initial Chebyshev array factor pattern of a 25-element antenna array designed for − 25 dB sidelobe level.

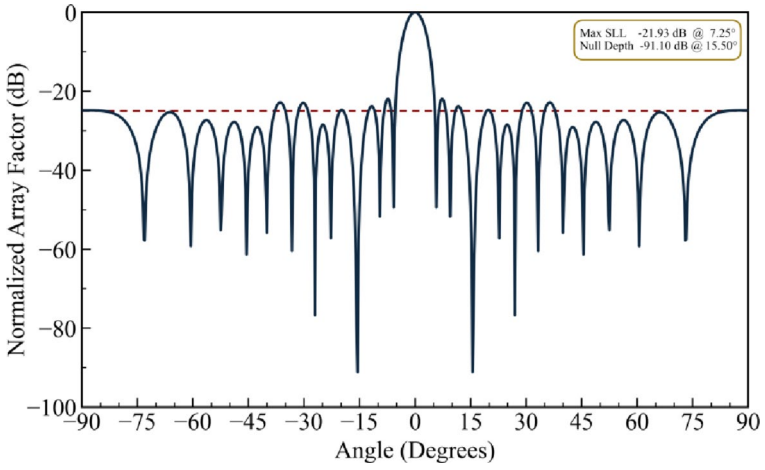


Fig. 3. The array factor exhibiting a single null with a depth of − 91.10 dB at 15.50°, corresponding to the third sidelobe.

$$\text{EMSL} = \begin{cases} 0, & if\ AF_o(\theta > 6^\circ) \leq MSL \\ 1, & \text{otherwise} \end{cases} \tag{5}$$

For this scenario, MSL is set to -21 dB and the weights w_1, w_2 and w_3 given in Eq. 2 were selected as 30, 20, and 0, respectively. The weight w_3 was set to 0 because the DRR value was not intended to be considered in this nulling process. The pattern obtained is shown in Fig. 3. The NDL, MSL and DRR values achieved with the presented method are − 91.1 dB, -21.9 dB, and 3.29, respectively.

In the subsequent example, to demonstrate the ease of adjusting the relative importance of the design parameters during the optimization process, only w_2 and w_3 were modified to 0 and 20, respectively. Accordingly, the array element amplitudes were re-optimized using the HFOSC algorithm based on these updated design parameters.

The resulting radiation pattern is shown in Fig. 4. For this case, the achieved NDL, MSL, and DRR are equal to − 94.5 dB, − 15.7 dB, and 1.78, respectively. As expected, even though the maximum sidelobe performance of the array pattern became worse than in the previous example, the DRR performance improved, reflecting the trade-off between the weighting factor values.

For a different example of the single nulling problem, the MSL given in Eq. 5 was constrained to -24 dB and the weighting values were set to those of the first example. As shown in Fig. 5, the MSL of the pattern is obtained as -24.8 dB, whereas in the first example it is -21.9 dB. In other words, an improvement of approximately 3 dB in the MSL was achieved.

In the final case of the single null steering problem, the value of NDL specified in Eq. 4 was constrained to -145 dB to achieve a deeper null. As illustrated in Fig. 6, the null depth was significantly enhanced from − 91.1

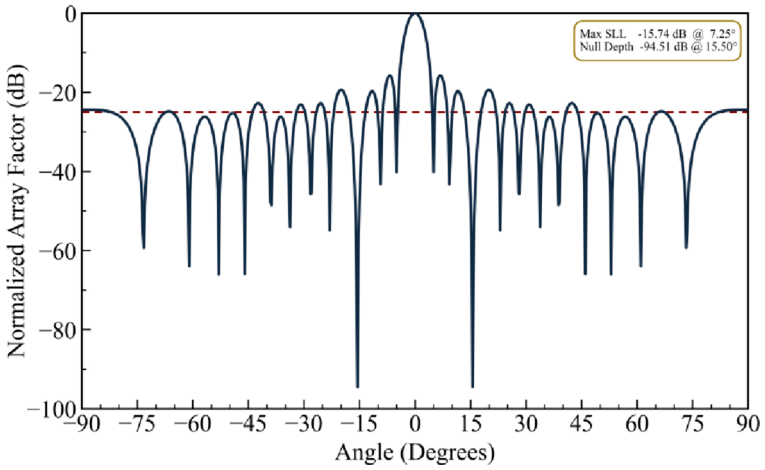


Fig. 4. The array factor exhibiting a single null at 15.50° under a constrained dynamic range ratio, emphasizing reduced excitation amplitude variation.

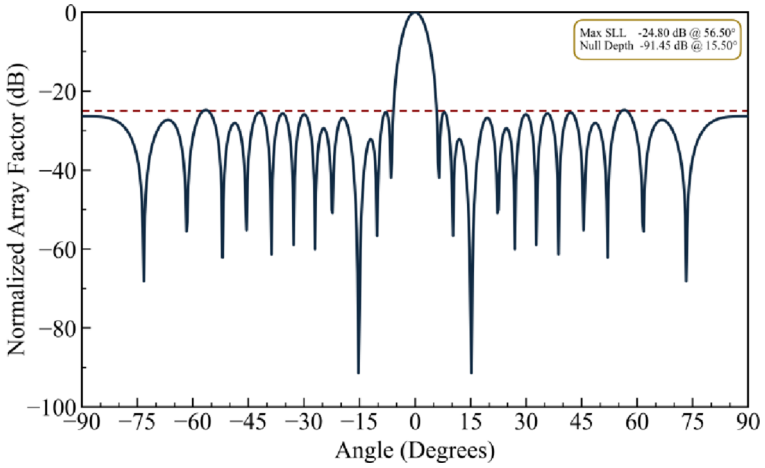


Fig. 5. The array factor exhibiting a single null at 15.50° under a constrained MSL, resulting in improved sidelobe suppression.

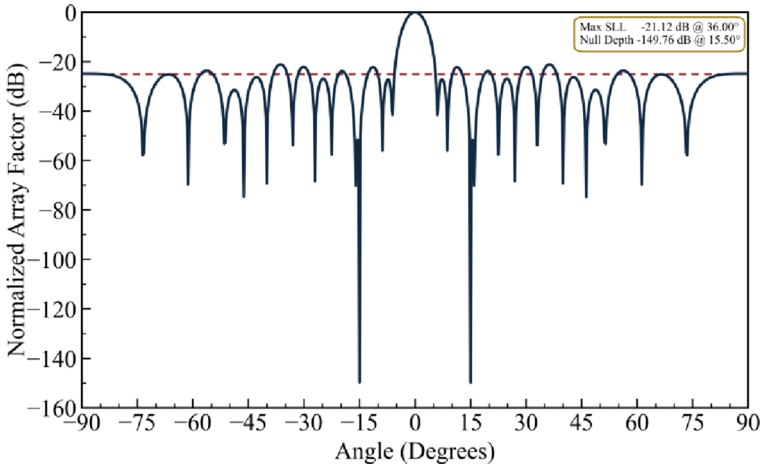


Fig. 6. The array factor exhibiting a single null at 15.50° under a constrained NDL, emphasizing enhanced null depth performance.

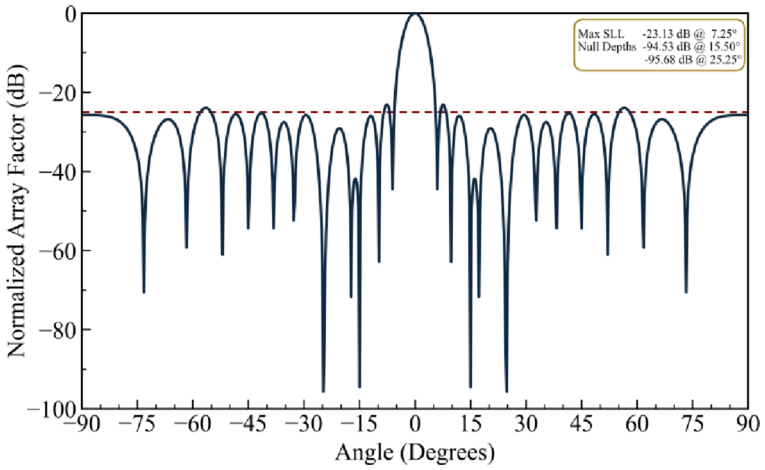


Fig. 7. The array factor exhibiting double nulls at 15.50° and 25.25°, corresponding to the third and fifth sidelobes.

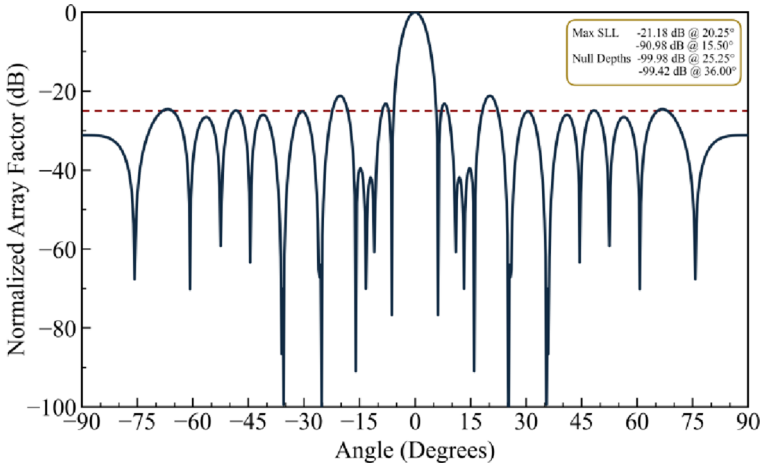


Fig. 8. The array factor exhibiting triple nulls at 15.50°, 25.25°, and 36.00°, corresponding to the third, fifth, and seventh sidelobes.

dB to -149.8 dB. However, since no constraints were applied to the DRR, its value increased from 3.29 in the first case to 3.49 in this scenario.

To demonstrate the effectiveness and ease of implementation of the HFOSC algorithm in multi-null steering problems, radiation patterns with dual and triple nulls are presented in the fifth and sixth examples, respectively. By modifying nulling angles θ_{na} given in Eq. 3 for the multi nulling purpose, in the fifth example, the initial pattern's third and fifth sidelobe peaks at 15.5° and 25.2° were successfully nullified, while in the sixth example, nulls were introduced at 15.5°, 25.2°, and 36.1° corresponding to the third, fifth, and seventh sidelobe peaks. The resulting radiation patterns with nulls at these specified angles are shown in Figs. 7 and 8, respectively. For both optimization scenarios, while no constraints were imposed on the DRR, the NDL and MSL were set to -90 dB and − 21 dB, respectively.

In the last example, a pattern with a broad null sector centered at 15.5° with $\Delta\theta = 4°$ is obtained. This corresponds to 2° on both sides of the center angle. The NDL value was selected as -65 dB within the range of [13.5 °, 17.5 °], and no restrictions were made for DRR and MSL. As shown in Fig. 9, a null depth of -69 dB is achieved across the specified spatial region.

It is clear from Figs. 3, 4, 5, 6, 7, 8 and 9 that this technique effectively determines the element amplitudes for an array pattern with single, multiple, and broad nulls imposed in the directions of interference, while maintaining the main beam and sidelobes close to the initial Chebyshev pattern. The synthesis results show fundamental trade-offs between competing design objectives. Comparing Figs. 3 and 4 illustrates the DRR-performance trade-off: limiting DRR to 1.78 enhances amplitude equalization at the expense of MSL, which degrades from − 21.9 dB to − 15.7 dB. This occurs because uniform excitation is an inherent restriction in pattern shaping. The null depth–sidelobe trade-off can be seen in Figs. 3 and 6: very deep nulls (NDL = − 149.8 dB) can be attained at the cost of increased DRR (3.49) and slightly reduced MSL (− 21.1 dB). On the other hand, the best

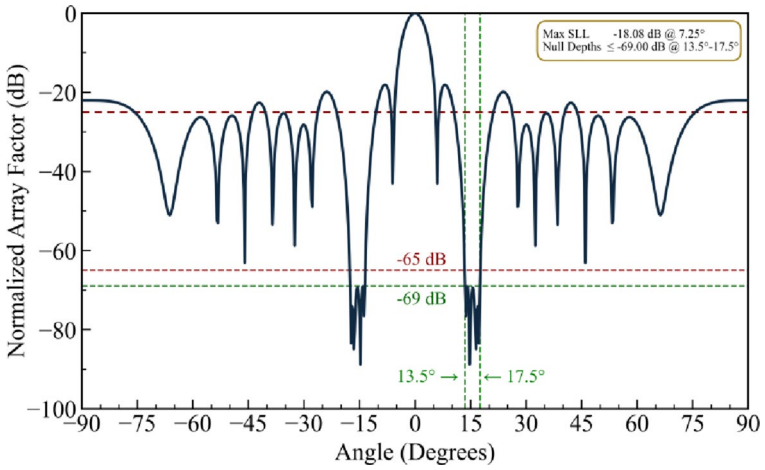


Fig. 9. The array factor exhibiting a broad null spanning the angular range of 13.50°–17.50°, corresponding to ± 2° around the center angle of 15.50°.

Index	Initial Chebyshev Pattern	Computed with HFOSC Algorithm						
n	Figure 2	Figure 3	Figure 4	Figure 5	Figure 6	Figure 7	Figure 8	Figure 9
0	1.00000	1.00000	1.00000	1.00000	1.00000	1.00000	1.00000	1.00000
± 1	0.99235	1.98637	1.77951	1.81013	1.81722	1.75909	1.81790	1.72900
± 2	0.96966	1.74856	1.46049	1.74662	1.68700	1.60401	1.31716	2.56725
± 3	0.93274	1.51821	1.39042	1.63411	1.42536	1.52538	1.50972	2.33831
± 4	0.88288	1.58384	1.31631	1.53210	1.31507	1.5524	1.60456	2.21082
± 5	0.82180	1.60180	1.40613	1.55123	1.47684	1.50556	1.54256	1.73877
± 6	0.75159	1.41777	1.72246	1.39394	1.15788	1.31195	1.44617	2.07746
± 7	0.67457	1.34180	1.65956	1.26327	1.10831	1.21614	1.33642	1.91501
± 8	0.59321	1.44589	1.50518	1.11303	1.25211	1.07316	0.88625	1.74144
± 9	0.51003	1.02928	1.23326	0.89940	0.86947	1.06088	0.75383	1.45643
± 10	0.42748	0.75718	1.03411	0.57542	0.60195	0.79345	0.69641	0.52051
± 11	0.34782	0.60446	1.00430	0.32224	0.52043	0.32624	0.36021	0.32797
± 12	0.66446	1.11091	1.51615	0.86889	1.08052	0.86135	0.78404	1.01751

Table 1. The Element Amplitudes Normalized According to Center Elements for Figs. 2, 3, 4, 5, 6, 7, 8 and 9.

sidelobe suppression (Fig. 5, MSL = − 24.8 dB) sacrifices null depths moderately. Multi-null cases (Figs. 7 and 8) and wide nulls (Fig. 9) impose even stronger constraints on the solution, demanding higher DRR (5.05 and 7.83, respectively) to meet additional angular conditions. These trade-offs arise from the limited degrees of freedom ($N = 25$ elements): each constraint reduces the flexibility available to optimize the others.

The above examples and results make it clear that changing the relative importance of key criteria for null steering designs, including MSL, NDL, and DRR, is straightforward. For example, much deeper nulls can be obtained at the cost of slight degradations in DRR and MSL. The use of weighting coefficients gives antenna designers great freedom and control over the synthesized radiation pattern. These parameters are critical in the formation of the pattern since they affect the excitation amplitude of each array element. Designers are frequently required to compromise between the theoretical ideal pattern and the practical limitations imposed by physical, electrical, and environmental constraints. By changing the weighting coefficients, a wide range of patterns can be generated and considered as approximations to the target pattern. In this way, weighting parameters can be systematically varied to design arrays with optimized performance for particular applications and with robustness against the inevitable imperfections of practical realizations.

The amplitudes of the array elements for Figs. 2, 3, 4, 5, 6, 7, 8 and 9 are shown in Table 1, and the values achieved for each example according to the design parameters of Main Lobe Width (MLW), Half-Power Beamwidth (HPBW), NDL, MSL, and DRR are reported in Table 2. It is also worth mentioning that the optimization based on HFOSC on the Python platform was conducted with a step (resolution) of 0.25° over the interval [0°, 90°]. All the example results obtained in the paper are quite satisfactory and require about 3–7 min on a computer with an Intel Core i5 10th Gen processor and 16 GB RAM. The element amplitudes obtained by the HFOSC algorithm for Figs. 3, 4, 5, 6, 7, 8 and 9 are evenly symmetric about the center of the array. The HPBW of the nulling patterns obtained by the HFOSC method is nearly equal to that of the original Chebyshev pattern. Moreover, the attained null depth and sidelobe level are also good. It can be seen that the patterns in

Figure	MLW (degree)	HPBW (degree)	NDL (dB)	DRR	MSL (dB)
2	6.00	4.65		2.875	-25.000
3	5.75	4.75	-91.096 @15.50°	3.286	-21.932
4	5.00	4.25	-94.508 @15.50°	1.780	-15.738
5	6.50	4.75	-91.450 @15.50°	5.617	-24.797
6	6.00	4.75	-149.762 @15.50°	3.492	-21.117
7	6.00	4.75	-94.529 @15.50° -95.677@25.25°	5.392	-23.133
8	6.25	4.75	-90.979 @15.50° -99.982 @25.25° -99.419 @36.0°	5.047	-21.180
9	6.00	4.75	-69.053 @13.50° -69.070 @14.00° -73.191 @14.50° -76.913 @15.00° -69.385 @15.50° -72.628 @16.00° -84.889 @16.50° -74.026 @17.00° -70.823 @17.50°	7.828	-18.082

Table 2. The Values for Each Example According to Design Criteria.

Figs. 3, 4, 5, 6, 7, 8 and 9 are symmetric on both sides of the main beam. This symmetry arises because the element amplitudes are symmetrically distributed about the center of the array.

For a $2N+1$ element array, the center element is taken as the reference for amplitude scaling and hence is not subject to attenuation. The amplitudes of the other N elements on one side of the array are varied independently, since the other side is the mirror image. Therefore, the total number of attenuators needed is effectively reduced to N.

Although strong practical advantages emerge from using amplitude-only control, the hardware realization of these patterns presents specific implementation challenges. First, due to amplitude quantization introduced by finite-bit attenuators, the optimized weights become discretized, which may degrade the achievable null depths. In particular, extremely deep nulls, such as the − 149.8 dB example shown in Fig. 6, are highly sensitive to amplitude quantization. In practical implementations, attenuators have a finite number of bits (e.g., 4- to 8-bit resolution). This forces the optimized continuous amplitude weights to be rounded to the nearest discrete levels. Such rounding can raise the effective null depth by tens of decibels. For instance, a theoretical null of − 149.8 dB may degrade to a practically achievable depth of only − 50 dB to − 70 dB, depending on the quantization resolution. Therefore, when designing for real-world systems, the required null depth must be balanced against the available hardware precision. For applications demanding very deep nulls, higher-resolution attenuators (e.g., 12-bit or more) or alternative techniques may be necessary. This trade-off between theoretical performance and hardware realizability should be carefully considered by system designers. Second, mutual coupling and embedded element patterns always differ from the ideal array factor, and compensation for this is normally accomplished by introducing full-wave coupling matrices into the optimization process. Additionally, physical limitations including DRR, amplifier nonlinearities, and component tolerances limit the realizable amplitude distributions. Not least among these deterministic factors, the method's resilience to uncertainties, such as manufacturing inaccuracies, element variations, and environmental noise, is paramount to dependable operation. As a result, future work will focus on incorporating these realistic constraints directly into the synthesis model and carrying out a comprehensive robustness study to guarantee performance under real-world operating conditions.

Comparative performance analysis

In this section, the results of the HFOSC algorithm are compared with those of popular metaheuristic algorithms such as the GA, PSO, and WOA. All algorithms are run with the same problem parameters, including the same antenna array configuration, identical coefficient bounds, and the same broadband suppression specification centered at 15.5° with a total suppression width of 4° (±2°). For statistical confidence, each algorithm is run independently 100 times with different random initial seeds.

To provide a clear and structured assessment, the comparison is presented from two complementary perspectives:

(i) optimization cost and convergence characteristics,

(ii) radiation pattern quality metrics reflecting physical antenna performance.

Table 3 shows the statistics of cost optimization at convergence together with the computational efficiency for all considered algorithms. HFOSC also has the smallest standard deviation (6.91), which corresponds to stable and repeatable convergence across different runs. This implies that HFOSC exhibits strong search stability and consistent performance. Although PSO attains several competitive best cost values, including one that is the best among all algorithms, its significantly higher standard deviation indicates unstable convergence and strong run-to-run variation. GA demonstrates fairly consistent performance but remains inferior to HFOSC in both average cost and convergence reliability. WOA shows the weakest performance, characterized by large mean cost and high variance, indicating poor exploitation capability for this problem. In terms of computational complexity,

Algorithm	Best Cost	Mean Cost	Std Cost	Mean Time (s)
HFOSC	49.19	58.44	6.91	3.34
GA	50.90	63.38	7.84	4.58
PSO	57.98	121.28	39.25	3.76
WOA	60.17	167.47	39.92	4.09

Table 3. Statistical comparison of optimization cost and computational performance over 100 independent runs.

Algorithm	Mean MSLL (dB)	Mean Min NDL (dB)	Mean Max NDL (dB)	Mean HPBW (deg)	Mean DRR	Best MSLL (dB)	Best Min NDL (dB)	Best Max NDL (dB)
HFOSC	−17.60	−71.83	−58.11	4.52	7.34	−19.14	−74.11	−59.27
GA	−17.89	−74.09	−57.57	4.50	7.35	−18.43	−71.63	−57.15
PSO	−18.21	−69.30	−46.46	4.62	7.45	−18.14	−70.46	−59.16
WOA	−17.58	−68.49	−38.30	4.68	7.18	−17.13	−71.14	−59.37

Table 4. Comparison of radiation pattern performance metrics obtained by different optimization algorithms.

HFOSC achieves equal or better performance with fewer function evaluations, which sufficiently demonstrates that HFOSC provides an effective balance between exploration and exploitation.

Although numerical optimization can be evaluated through cost-based metrics, this does not fully represent the physical quality of the produced radiation patterns. Therefore, important electromagnetic performance indicators such as MSLL, NDL, HPBW, and DRR are given in Table 4. HFOSC achieves a reasonably well-balanced suppression pattern in terms of an average minimum NDL of − 71.83 dB and a relatively low maximum NDL (− 58.11 dB). This means that the suppression is not only deep but also exhibits good flatness across the entire NDL. In addition, the average HPBW of 4.52° confirms that the MLW remains close to the original one without obvious broadening. GA achieves similar NDL in some cases but with slightly larger variation in null uniformity. PSO, while producing good sidelobe suppression in isolated runs, appears to be less consistent within the NDL, showing higher maximum NDL. Among the methods under comparison, WOA has the worst performance, with much shallower null suppression and a wider main lobe. The DRR also shows that HFOSC produces physically realizable solutions with moderate excitation levels and that no extreme scaling of coefficients, which might prevent practical realization, takes place. To illustrate the quantitative nature of these trade-offs, when the DRR constraint is tightened by reducing the DRR weighting coefficient, DRR decreases from 3.29 to 1.78 — a reduction of 45.9% — while the MSL degrades from − 21.9 dB to − 15.7 dB (a deterioration of 6.2 dB), demonstrating that amplitude uniformization imposes a significant cost on sidelobe control. This quantitative trade-off analysis provides practical guidance for designers in selecting appropriate weighting coefficients according to system-level priorities.

Broadly, the comparative results of Tables 3 and 4 indicate that HFOSC is more robust and balanced in optimization performance when compared with the other metaheuristics. Although some algorithms may produce competitive results in certain individual criteria, HFOSC consistently achieves stable convergence and good broadband suppression which makes it a strong candidate for broadband null-steering antenna array synthesis. To further validate the statistical significance of the observed performance differences, the Wilcoxon rank-sum test was applied to the optimization results obtained from 100 independent runs. The test results confirm that the differences in optimization cost between HFOSC and PSO, as well as between HFOSC and WOA, are statistically significant ($p < 0.05$), thereby providing rigorous statistical support for the superiority of the proposed algorithm.

Figure 10 illustrates the comparative convergence characteristics of HFOSC against GA, PSO, and WOA, clearly demonstrating the superior efficiency of the proposed algorithm. The HFOSC curve exhibits a significantly sharper and more rapid descent in the cost function value compared to the other metaheuristics, indicating a faster convergence speed. Unlike the competing algorithms, which show slower progress or premature stagnation, HFOSC effectively balances exploration and exploitation to quickly locate the global optimum. This behavior confirms that the algorithm requires fewer iterations to achieve high-quality solutions, thereby reducing the overall computational burden while maintaining robust and stable performance throughout the optimization process.

Conclusions

In the conventional problem of radiation pattern synthesis subject of nulling constraints where it is simply desired to null out a number of interference sources, it is now well known that the synthesis of the antenna pattern boils down to the formation of deep nulls in the suitable directions of arrival of the interfering signals. The proposed HFOSC algorithm is an efficient method to synthesize antenna array patterns with exact nulls at the given directions via only amplitude control of array elements. Thus, the new pattern may be considered to be 'close' to the original Chebyshev reference pattern. The presented results highlight the inherent trade-

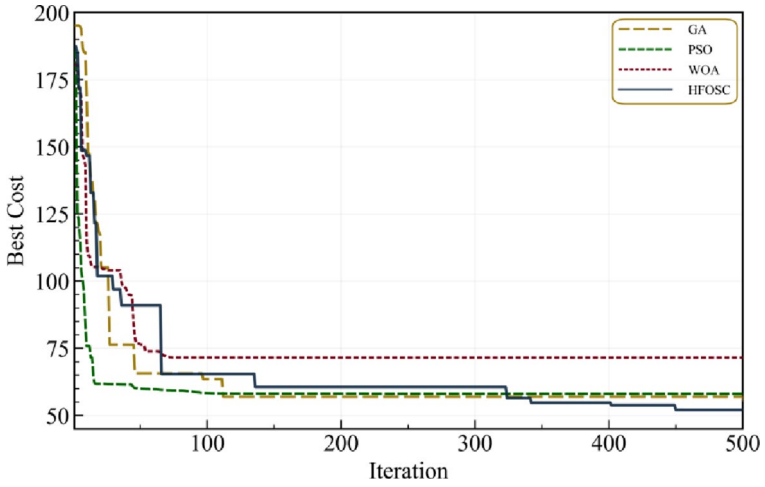


Fig. 10. Comparative convergence performance of HFOSC, GA, PSO, and WOA algorithms in terms of the mean best-so-far cost averaged over independent runs.

offs between NDL, SLL, and DRR. For example, deeper nulls (such as −149.8 dB) may require higher DRR values, which can make the hardware more difficult to realize due to a larger amplitude dynamic range. On the other hand, limiting the DRR (e.g., to 1.78) enhances the realizability of the solution but may degrade the null depth and increase the MSL. These parameters need to be balanced by designers according to system priorities, such as deep nulling for interference suppression, low MSL for coverage uniformity, and moderate DRR for hardware simplicity. The weighting coefficients ($w?$, $w?$, $w?$) in the cost function provide a convenient means for systematically exploring these trade-offs. For instance, designers should select the weighting factors based on application priorities, emphasizing $w?$ for anti-jamming (deep nulls), $w?$ for spectral coexistence (low MSL), or $w?$ for cost-sensitive implementations (low DRR).

For demonstration purposes, although the examples consider a half-wavelength spaced linear array of isotropic elements, it is clear from the fundamental synthesis concepts presented that the HFOSC technique is suitable for many other geometry configurations and is not restricted to this specific array type. The basic optimization framework can be straightforwardly generalized to planar arrays employed in massive MIMO systems, as well as to circular and conformal configurations for platform-based radars. The procedure also allows for sparse and non-uniform arrays for aperture thinning and can easily include the embedded patterns of practical directive elements such as patches or dipoles. Such built-in adaptivity means that the amplitude-only approach is a strong candidate for high-performance pattern synthesis in a range of future wireless and sensing systems, including 5G/6G and radar, in which energy-efficient hardware and real-time adaptation to interference remain vital.

Data availability

All data generated or analyzed during this study are included in the manuscript.

Received: 1 January 2026; Accepted: 6 April 2026
Published online: 10 April 2026

References

1. Rosic, Z., Mihic, O., Aleksic, D. & Drajic, D. Novel method for optimal synthesis of 5G millimeter wave linear antenna array. *Int. J. Antennas Propag.* **2017** (6848234), 1–9. https://doi.org/10.1155/2017/6848234 (2017).
2. Vankayalapati, S. & Pappula, L. Linear antenna array optimization for beamforming and null steering in 6G wireless systems using a modified cat swarm optimization algorithm. *Phys. Scr.* **100** https://iopscience.iop.org/article/10.1088/1402-4896/ae1f46/meta (2025).
3. Al Ka'bi A. A Proposed Method for Synthesizing the Radiation Pattern of Linear Antenna Arrays. *J. Commun.* **17**, 7, 553–558. https://doi.org/10.12720/jcm.17.7.553-558 (2022).
4. Al Ka'bi, A. & Mustafa, A. Design of MIMO Antenna for Wideband THz Mobile Communications. *Telecommunications Radio Eng.* **83**, 8. https://doi.org/10.1615/TelecomRadEng.2024051220 (2024).
5. Aljaf, D. A. & Mohammed, J. R. Multiple antenna array patterns reconfiguration with common excitation amplitudes and optimized phases. *J. Eng. Sci. Technol.* **18**, 2, 1199–1208 (2023).
6. Albagory, Y. & Alraddady, F. An efficient adaptive and steep-convergent sidelobes simultaneous reduction algorithm for massive linear arrays. *Electronics* **11**, 2, 170. https://doi.org/10.3390/electronics11020170 (2022).
7. Bhattacharyya, K. Wide-band pattern nulling in phased array and phased array-fed reflector antennas. *Prog Electromagn. Res. C.* **153**, 149–157. https://doi.org/10.2528/PIERC25012001 (2025).
8. Adriansyah, M. A., Wahdiyat, A. I., Fitri, I. R., Murad, N. A. & Apriono, C. Sidelobe level suppression in linear and planar phased arrays using grey wolf optimization with local search refinements. *IEEE Access.* **13**, 27818–27832. https://doi.org/10.1109/ACCESS.2025.3540456 (2025).
9. Wang, S. T. & Zhu, L. Proposal and design of a null reconfigurable patch antenna on the basis of multimode method. *IEEE Trans. Antennas Propag.* **71**, 8, 6286–6296. https://doi.org/10.1109/TAP.2023.3276512 (2023).

10. Guney, K. & Akdagli, A. Null steering of linear antenna arrays using a modified tabu search algorithm. *Prog Electromagn. Res.* **33**, 167–182 (2001).
11. Recioui, A. Application of the Spiral Optimization Technique to Antenna Array Design. In *Handbook of Research on Emergent Applications of Optimization Algorithms* **2**, 364–385 (2017).
12. Guney, K., Babayigit, B. & Akdagli, A. Position-only pattern nulling of linear antenna array by using a clonal selection algorithm. *Electr. Eng.* **90**, 2, 147–153. https://doi.org/10.1007/s00202-006-0056-9 (2007).
13. Recioui, A. & Bentarzi, H. Null steering of Dolph-Chebychev arrays using Taguchi method. *WSEAS Trans. Commun.* **9** (11), 720–729 (2010).
14. Recioui, A. & Bentarzi, H. Pattern nulling of linear array antennas with mutual coupling effects using taguchi method. In *2012 24th IEEE International Conference on Microelectronics (ICM),* 1–4 (2012).
15. Kadhim, M. A. Null steering using phase shifters. *ARPN J. Eng. Appl. Sci.* **13**, 3045–3051 (2018).
16. Liang, J., Fan, X., Fan, W., Zhou, D. & Li, J. Phase-only pattern synthesis for linear antenna arrays. *IEEE Antennas Wirel. Propag. Lett.* **16**, 3232–3235. https://doi.org/10.1109/LAWP.2017.2771380 (2017).
17. Raghuvanshi, A. & Alraddady, F. Linear antenna array pattern synthesis using multi-verse optimization algorithm. *Electronics* **13,** 17, (3356). https://doi.org/10.3390/electronics13173356 (2024).
18. Jin, X. R., Zhang, Q., Kong, L. B., Ding, G. W. & Wang, S. Y. Wide null steering of realistic antenna array. *Results Eng.* **26**, 105038. https://doi.org/10.1016/j.rineng.2025.105038 (2025).
19. He, J., Cheng, Z., He, Z. & Yuan, K. Phase-only transmit beampattern design for large phased array antennas with multi-point nulling. *Multidimens Syst. Signal. Process.* **33**, 2, 597–619. https://doi.org/10.1007/s11045-021-00815-7 (2022).
20. Chakraborty, A. et al. Optimal design of smart antenna arrays for beamforming, direction finding, and null placement using soft computing methods. *Int. J. Numer. Model. Electron. Netw. Devices Fields.* **37** (6), 1–13. https://doi.org/10.1002/jnm.3302 (2024).
21. Zhang, Y. et al. Array nulling synthesis based on hyper-parameter optimized self-paced learning convolutional neural networks. *IEEE Trans. Antennas Propag.* **72**, 6, 5325–5330. https://doi.org/10.1109/TAP.2024.3378385 (2024).
22. Zhao, Z., Zhao, H., Wang, Z., Zheng, M. & Xun, Q. Radial basis function neural network optimal modeling for phase-only array pattern nulling. *IEEE Trans. Antennas Propag.* **69**, 11, 7971–7975. https://doi.org/10.1109/TAP.2021.3083787 (2021).
23. Zhao, Z., Zhao, H., Zheng, M. & Tang, J. Real-time phase-only nulling based on deep neural network with robustness. *IEEE Access.* **7**, 142287–142294. https://doi.org/10.1109/ACCESS.2019.2943420 (2019).
24. Kumar, S. & Singh, H. Antenna array pattern synthesis using nature-inspired computational techniques: A review. *Arch. Comput. Methods Eng.* **30**, 5, 2441–2475. https://doi.org/10.1007/s11831-023-09900-5 (2023).
25. Lin, Y. D., Chang, J. H. & Lai, Y. C. Deep reinforcement learning-based adaptive nulling in phased array under dynamic environments. *IEEE Access.* **13**, 130988–131002. https://doi.org/10.1109/ACCESS.2025.3591643 (2025).
26. Luyen, V. T. & Giang, T. V. B. Null-steering beamformer using bat algorithm. *Appl. Comput. Electromagn. Soc. Newsl.* **33**, 1, 23–29 (2018).
27. Poddar, S., Paul, P., Chakraborty, A., Ram, G. & Mandal, D. Design optimization of linear arrays and time-modulated antenna arrays using meta-heuristics approach. *Int. J. Numer. Model. Electron. Netw. Devices Fields.* **35** (5), 1–18. https://doi.org/10.1002/jnm.3010 (2022).
28. Dutta, K. P., Misra, B. & Mahanti, G. K. Meta-heuristic optimization algorithms for placement of multiple nulls and minimization of side lobe level in quadrant symmetric sparse array antenna. *Int. J. Commun. Syst.* **35, 10**, (e5149), 1–15. https://doi.org/10.1002/dac.5149 (2022).
29. Raghuvanshi, A., Sharma, A. & Awasthi, A. K. Pattern synthesis of linear antenna array using chaos game optimization algorithm. *COMPEL* **44**, 6, 900–913. https://doi.org/10.1108/COMPEL-12-2024-0549 (2025).
30. Sharma, R. Antenna array pattern synthesis using metaheuristic algorithms: A review. *IETE Tech. Rev.* **40**, 1, 90–115. https://doi.org/10.1080/02564602.2022.2051616 (2023).
31. Durmus, H., Kurban, R. & Karakose, E. A comparison of swarm-based optimization algorithms in linear antenna array synthesis. *J. Comput. Electron.* **20**, 4, 1520–1531. https://doi.org/10.1007/s10825-021-01711-w (2021).
32. Tong, L. V., Kha, K. M., Nguyen, C. V., Nguyen, T. L. & Truong, G. B. V. Null-steering beamformers for suppressing unknown direction interferences in sidelobes. *J. Commun.* **17**, 8, 600–607. https://doi.org/10.12720/jcm.17.8.600-607 (2022).
33. Vegesna, N., Yamuna, G. & Kumar, T. S. A comprehensive study of linear antenna arrays using nature-inspired algorithms. *Lect Notes Electr. Eng.* **827**, 403–410. https://doi.org/10.1007/978-981-16-8554-5_38 (2022).
34. Lale, T., Yüksek, G. & Çınar, R. F. A novel hybrid metaheuristic for optimizing deep CNN hyperparameters to enhance heart disease prediction on a comprehensive merged dataset. *Cluster Comput.* **29**, 117. https://doi.org/10.1007/s10586-025-05892-y (2026).
35. Jabari, M. et al. A robust multi-stage FOPI(1 + PIDn) controller for precision control of switched reluctance motors under nonlinear and uncertain conditions. *Energy Rep.* **15**, 109231. https://doi.org/10.1016/j.egyr.2026.109231 (2026).
36. Ekinci, S. et al. Reliable parameter estimation of nonlinear chaotic systems and PMSMs with the stellar oscillation optimizer. *Sci. Rep. Mar.* https://doi.org/10.1038/s41598-026-41940-2 (2026).
37. Özmen, H., Izci, D., Rizk-Allah, R. M., Ekinci, S. & Dalarsson, M. Optimization of split-ring resonator slots using levy-opposition-enhanced Newton Raphson method for high-gain UWB Vivaldi antenna design. *Sci. Rep.* **16** (1), 7828. https://doi.org/10.1038/s41598-026-41244-5 (2026).
38. Yetgin, Z. & Şamdan, M. Honey formation optimization: HFO. *Turk. J. Eng.* **5**, 2, 81–88. https://doi.org/10.31127/tuje.693103 (2021).
39. Yetgin, Z. & Ercan, U. Honey formation optimization with single component for numerical function optimization: HFO-1. *Neural Comput. Appl.* **35**, 24897–24923. https://doi.org/10.1007/s00521-023-08984-1 (2023).
40. Ercan, U., Boyar, I., Kilic, T. O., Yetgin, Z. & Ertekin, C. Parameter optimization of drying models using honey formation optimization-1 (HFO-1). *Food Bioprod. Process.* **154**, 392–401. https://doi.org/10.1016/j.fbp.2025.09.016 (2025).

Acknowledgements

Thanks to all the reviewers and editors for their valuable comments and assistance with this paper.

Author contributions

All authors contributed equally.

Declarations

Competing interests

The authors declare no competing interests.

Additional information

Correspondence and requests for materials should be addressed to D.I. or M.R.

Reprints and permissions information is available at www.nature.com/reprints.

Publisher's note Springer Nature remains neutral with regard to jurisdictional claims in published maps and institutional affiliations.

Open Access This article is licensed under a Creative Commons Attribution-NonCommercial-NoDerivatives 4.0 International License, which permits any non-commercial use, sharing, distribution and reproduction in any medium or format, as long as you give appropriate credit to the original author(s) and the source, provide a link to the Creative Commons licence, and indicate if you modified the licensed material. You do not have permission under this licence to share adapted material derived from this article or parts of it. The images or other third party material in this article are included in the article's Creative Commons licence, unless indicated otherwise in a credit line to the material. If material is not included in the article's Creative Commons licence and your intended use is not permitted by statutory regulation or exceeds the permitted use, you will need to obtain permission directly from the copyright holder. To view a copy of this licence, visit http://creativecommons.org/licenses/by-nc-nd/4.0/.

© The Author(s) 2026